# Starburst amacrine cells amplify optogenetic visual restoration through gap junctions

Yusaku Katada[1,2], Hiromitsu Kunimi[1,2], Kenta Kobayashi[3], Hideyuki Okano[4], Kenji F. Tanaka[5], Kazuo Tsubota[2], and Toshihide Kurihara[1,2].

[1]Laboratory of Photobiology, [2]Department of Ophthalmology, [4]Department of Physiology, [5]Department of Neuropsychiatry, Keio University School of Medicine, Shinanomachi, Shinjuku-ku, Japan

[3]Section of Viral Vector Development, Center for Genetic Analysis of Behavior, National Institute for Physiological Sciences, National Institutes of Natural Sciences, Okazaki, Aichi, Japan

**Corresponding authors:**

Toshihide Kurihara, MD/PhD

Laboratory of Photobiology, Department of Ophthalmology, Keio University School of Medicine; 35 Shinanomachi, Shinjuku-ku, Tokyo 160-8582, Japan

Tel.: +81-3-5363-3204, Fax: +81-3- 5363-3274

E-mail: kurihara@z8.keio.jp

19 Kazuo Tsubota, MD/PhD

20 Professor and Department Chair, Department of Ophthalmology, Keio University School of

21 Medicine; 35 Shinanomachi, Shinjuku-ku, Tokyo 160-8582, Japan

22 Tel.: +81-3-5363-3269, Fax: +81-3- 3358-5961

23 E-mail: tsubota@z3.keio.jp

**Abstract**

**Ectopic induction of optogenetic actuators, such as channelrhodopsin, is a promising approach to restore vision in the degenerating retina. However, the cell type-specific response of ectopic photoreception has not been well understood. It is not easy to obtain efficient gene expression in a specifically targeted cell population by a transgenic approach. In the present study, we established retinal ganglion cell (RGC)- and amacrine cell gene induction in a murine model with high efficiency using an improved tetracycline transactivator-operator bipartite system (KENGE-tet system). To investigate the cell type-specific visual restoration effect, we expressed the channel rhodopsin gene into RGCs and amacrine cells using this system. Then, enhancement of the visual restoration effect was observed by gene transfer not only to RGCs but also to starburst amacrine cells. It was suggested that photoresponse from amacrine cells enhanced the maintained response of ganglion cells and furthered the visual restoration effect.**

## Introduction

Inherited retinal degeneration is one of the major causes of vision loss. More than 2 million people worldwide are blind due to this disease [1], and there is still almost no effective treatment. Previous studies have reported visual restoration effects in animal models using various molecules as optogenetic actuators [2–9]. In addition, clinical trials have also started using channelrhodopsin 2 (RST-001, ClinicalTrials.gov Identifier: NCT01648452), and Chrimson R (GS-030, ClinicalTrials.gov Identifier: NCT03326336), with gene transduction into RGCs by intravitreal injection of recombinant adeno-associated virus (rAAV). Although the visual reconstruction effects by optogenetic gene transfer, such as channelrhodopsin-2 into RGCs [10] and ON-bipolar cells [3,5,6,8,11], have been shown, interactions between other types of cells in the retinal neural circuits in optogenetic visual restoration have not between well understood. Channelrhodopsin 2 conductance was reported to be 50–250 fS [12], indicating the need for sufficient gene expression to control the membrane potential. In this study, we employed a tetracycline-controllable gene expression system (tet system) [13] in which the amount of gene expression has been much improved (KENGE-tet system) [14], and we established sufficient gene induction in RGCs and amacrine cells simultaneously. To investigate cell type-specific visual restoration effects, channelrhodopsin2(E123T/T159C) was ectopically expressed into these cells by this system.

58 Then, we revealed that amacrine cells played a role in retinal neuronal circuits via gap
59 junctions to enhance the optogenetic visual restoration effect.
60
61 **Results**
62 **Gene induction of RGCs and SACs in M4-YC and RGCs in 5B-YC**
63 We employed two different mouse lines that express the gene encoding the tetracycline
64 transactivation (tTA) protein under the control of a cell-type-specific promoter, muscarinic
65 acetylcholine receptor 4 (*Chrm4*)[15] or 5-hydroxytryptamine (5-HT, serotonin) 5B receptor
66 (*Htr5b*)[14] control region: *Chrm4*-tTA or *Htr5b*-tTA. These mice were further crossed with
67 another transgenic mouse line containing the yellow Cameleon-Nano 50 (YC) fluorescent
68 gene connected into the downstream of the tet operator (tetO) promoter [16]. The YC gene
69 expression was induced only by the presence of tTA protein in the double transgenic mice
70 (*Chrm4*-tTA::tetO-YC (M4-YC) or *Htr5b* -tTA::tetO-YC (5B-YC)) (Figure S1A, B). The
71 expression of YC was observed in the double transgenic mouse retina with a fluorescence
72 microscope. In the M4-YC mouse retina, we identified the expression of YC in RGCs
73 (Figure 1A-D, Figure S2A-E) and amacrine cells (Figure 1A-D, Figure S1E-F) with *in vivo*
74 fluorescence microscopy and in sections. In the 5B-YC mouse retina, we identified the
75 expression of YC in RGCs (Figure 1E-H) and the corneal stromal layer (Figure S2G-M)
76 with *in vivo* fluorescence microscopy and in sections. In both lines, no expression was found

77 in displaced amacrine cells, only RGCs were labeled in the ganglion cell layer, and the
78 percentage of YC-positive cells in RGC marker RBPMS [17]-positive cells was 35.4% (n=5)
79 in M4-YC and 36.5% (n=5) in 5B-YC from RGCs, which were equivalent (Figure 1I-L, O-
80 R, Figure S2M-Q). All of the amacrine cell expression in the M4 line was choline
81 acetyltransferase (ChAT) staining-positive and consisted of starburst amacrine cells (SACs)
82 (Figure 1M-T, Figure S3 A-L).
83
84 As a visual restoration model, the *Chrm4*-tTA and *Htr5b*-tTA line were crossed with tetO-
85 channelrhodopsin2(E123T/T159C) (tetO-ChR2) mice [18] (Figure S1C). *Chrm4*-tTA::tetO-
86 ChR2 (M4-ChR2) drove ChR2 expression in both RGCs and amacrine cells and *Htr5b* -
87 tTA::tetO-ChR2 (5B-ChR2) only in RGCs in the retina. In the retinas of these double
88 transgenic mice, photoreceptor degeneration was induced by intraperitoneal injection of N-
89 methyl-N-nitrosourea (MNU) [19]. MNU is an alkylating agent that causes DNA methylation
90 in the O6 position of guanine, resulting in apoptosis, and it has been widely used to induce
91 a pharmacological animal model of retinitis pigmentosa (RP). Two weeks after 75 mg/kg
92 MNU administration into the mice at the age of 8 weeks, the outer nuclear layer containing
93 photoreceptors was largely absent (Figure S4A, B), and the light-evoked response from
94 photoreceptors was not detected by electroretinography (ERG) (Figure S4C).

95 **M4-ChR2 mouse shows higher visual restoration effect.**

96 To evaluate the function of the channelrhodopsin ectopically induced in the transgenic
97 mouse retinas, we performed multi-electrode array (MEA) recording, which can record
98 extracellular potentials of RGCs (Figure S4D). As a result of photoreceptor degeneration
99 induced with MNU treatment, the control retina without channel-rhodopsin expression
100 (tetO-ChR2) showed no response from RGCs detected by MEA (Figure 2A). In contrast,
101 the M4-ChR2 (Figure 2B) and 5B-ChR2 (Figure 2C) retinas showed obvious light-induced
102 responses. After filtering with the Gaussian function (Figure 2D, E), the maintained
103 response after the peak was significantly greater in M4-ChR2 mice than in 5B-ChR2 mice
104 (Figure 2F), indicating that the light-evoked ON response in RGCs could be modified
105 through the response from amacrine cells.

106

107 To investigate whether light reception on the retina is transmitted to the visual cortex, we
108 then examined visual evoked potentials (VEPs) from the visual cortex (Figure 2G). The
109 output from the retinal ganglion cells is sent through the axons of the retinal ganglion cells
110 (optic nerve) to the lateral geniculate nucleus (LGN) of the thalamus, which is a region of
111 the mesencephalon, from the LGN to the primary visual cortex (V1) in the occipital lobe of
112 the cerebral cortex. VEPs were not detected in the control tetO-ChR2 mice with MNU

113 treatment (Figure 2H, I). In contrast, VEPs were observed in both M4-ChR2 and 5B-ChR2
114 mice treated with MNU (Figure 2H, I). In response to the light stimulus at 4000 cds/$m^2$, the
115 average of the VEP amplitude in MNU-treated M4-ChR2 mice was significantly higher
116 (143.6 μV; n=12, P=0.03) than in MNU-treated 5B-ChR2 (79.6 mV; n = 12) and the same
117 level as in the mice without MNU treatment (155 μV; n=4). However, the shapes of the
118 waveforms were irregular in both models compared to controls, and their physiological roles
119 are unknown. Thus, there is a limitation in this direct comparison.
120
121 To validate the model system, we examined the MEA, ERG and VEP of M4-ChR2 and 5B-
122 ChR2 in the absence of retinal degeneration (no MNU treatment and no mutation) as well.
123 As a result of MEA, the peak response was significantly reduced in both lines and was
124 further significantly reduced with MNU treatment (Figure S4E). A similar trend was
125 observed for the maintained response, whereas it was maintained in the M4 line (Figure
126 S4F). This finding suggests that channelrhodopsin gene induction into healthy RGCs
127 interferes with the physiological retinal light response. In addition, in the control mice, not
128 only the ON response but also the OFF response was confirmed. In contrast, the OFF
129 response was significantly lost in the M4 line (Figure S4H). It is known that SACs in the
130 INL are connected to off bipolar cells [20], which might be related to this change. As a result

131 of ERG and VEP, both lines tended to have shorter latencies, especially in photopic
132 examinations (Figure S5E, I, L, O), likely because of the channelrhodopsin response to
133 strong light [9] and its photoreception in RGCs resulting in short latency [21]. Although the
134 amplitude of both ERG and VEP tended to be small in the 5B line (Figure S5C, G, M, N),
135 these measurements were not significant, and there was no significant change in the shape
136 of the waveforms.
137
138 Next, light-dark transition testing (LDT) was performed to investigate whether ectopic
139 expression of channelrhodopsin in degenerative retinas leads to behavioral changes
140 according to visual restoration. Rodents tend to stay in dark places according to their visual
141 function since they are nocturnal and feel uneasy in bright environments (Figure 2J), while
142 the visually disturbing MNU-treatment (Figure 2K) resulted in almost half of the staying
143 time in bright and dark places (ratio in bright half at 10 min was closer to 0.5). In contrast,
144 both the M4-ChR2 and 5B-ChR2 mouse lines with each MNU-treatment showed decreased
145 staying time in bright places, indicating that visual restoration was confirmed in these
146 models. Furthermore, M4-ChR2 mice showed significantly higher visual restoration effects
147 than 5B-ChR2 mice (Figure 2K).
148 We also examined the optokinetic response (OKR) to investigate whether light receptivity

149 in the retina restored by ectopic channelrhodopsin expression led to central reflex movement
150 output. In OKR, a rotating striped pattern was displayed to the head-fixed mice to induce
151 eye movements, and the velocity was measured to evaluate the integrity of the subcortical
152 reflex circuitry of the mice (Figure S6A). OKR was not detected in the mice with MNU
153 administration except for the M4 line (4.80 deg/sec, n=6) (Figure S6B).
154 This outcome seems to be due to lack of ChR2 expression in SACs, which play a key role
155 in OKR [22], in the retinas of 5B-ChR2 mice. We also examined *rd1* mice as a genetic animal
156 model of RP. These mice have a nonsense mutation in the *Pde6b* gene leading to rapid
157 degeneration of rod, photoreceptors followed by loss of cones [23,24]. We used blind *rd1*
158 mutation mice at the age of 10-12 weeks for the following experiments. In the cases of *rd1*
159 mutant mice, no detectable OKR was observed in any combinations with each transgenic
160 line, including M4-ChR2. To investigate the dissociation of OKR between the MNU-
161 treatment and *rd1* models, the retinal thickness was compared under the conditions used for
162 the experiment. As a result, the total retinal thickness of *rd1* mice (78.3 μm; n=9) was
163 significantly thinner than that of MNU-treated mice (97.2 μm; n=10) evaluated on optical
164 coherence tomography (OCT) (Figure S6C, D). This outcome was thought to be because
165 the inner retinal layer was thinner of the *rd1* mouse (Figure S6E). Indeed, the inner nuclear
166 layer of the *rd1*, *rd1*;5B-ChR2 and *rd1*;M4-ChR2 mice was significantly thinner than that

167 of the MNU-treated mice (Figure S6F), suggesting that SACs in the inner layer were
168 degenerated. This result suggests that residual INL thickness and its durability might be
169 potential limitations of optogenetic gene therapy in inherited retinal disease patients
170 clinically.
171
172 **Acetylcholine and gap junctions were involved in the maintained response.**
173 The M4-ChR2 mouse line, which showed transgene expression in amacrine cells in addition
174 to RGCs, showed a higher maintained response and more effective visual restoration (Figure
175 2) than the 5B-ChR2 mice. Therefore, we investigated the neurocircuit pathway responsible
176 for the enhanced response due to amacrine cells using neurotransmitter blockers on the MEA
177 recording. Administration L-2-amino-4-phosphonobutyric acid (L-AP4), which is an
178 agonist for group III metabotropic glutamate receptors, including mGluR6 working as a
179 blocker of retinal ON-bipolar cells, did not show significant changes in either MNU-treated
180 M4-ChR2 (Figure 3A-C) or 5B-ChR2 (Figure 3D-F) retinas, indicating that the
181 photoresponse was not derived from photoreceptors. In contrast, administration of
182 mefenamic acid (MFA) or carbenoxolone, an inhibitor of gap junctions, induced a
183 significant decrease in the maintained response but not the peak of the response in the MNU-
184 treated M4-ChR2 retina (Figure 3G-I, Figure S7A-C). This change was recovered after

185 washout and not observed in the 5B-ChR2 retina (Figure S7D-F). SACs release GABA and
186 acetylcholine [25]. Thus, we also examined an inhibitor of GABA receptor (1,2,5,6-
187 tetrahydropyridin-4-yl) methylphosphinic acid (TPMPA), and a cholinergic antagonist,
188 atropine. As a result, no significant change was observed with administration of TPMPA
189 (Figure S7G-I), but atropine administration showed a similar decrease in maintained
190 response and in peak response in the MNU-treated M4-ChR2 mice (Figure 3J-L). In
191 addition, to determine whether this change occurred via bipolar cells, an AMPA receptor
192 antagonist, 6-cyano-7-nitro-quinoxaline-2,3-dione (CNQX), and an NMDA receptor
193 antagonist, D(-)-2-amino-5-phosphonopentanoic acid (D-AP5), were administered. As a
194 result, no statistically significant difference was observed, although there was a tendency
195 toward a decrease in the maintained response (Figure S7J-L). SACs form synapses with
196 bipolar cells, RGCs, and other amacrine cells [25–27]. It is also known that amacrine cells are
197 directly connected with RGCs through gap junctions [28,29], regulating neural circuits in the
198 retina [30]. Therefore, these results indicated that SACs enhanced the maintained response of
199 RGCs directly or indirectly through acetylcholine and gap junctions.
200
201 MEA showed a visual restoration effect induced by ectopic ChR2 expression in the
202 degenerative retina (Figure 2). These photoresponses obtained from MEA were all ON
203 responses, as previously reported [10313233]. Several slow photoresponses obtained from RGCs

204 were considered to have an ipRGC origin [34], and they were excluded from the data. The
205 MNU-treated M4-ChR2 retina showed a significant larger response in the maintained time
206 phase compared to 5B-ChR2. As a result of a neurotransmitter blocking test (Figure 4),
207 inhibition of acetylcholine and gap junctions decreased the maintained response of only M4-
208 ChR2 retinas. The difference between M4-ChR2 and 5B-ChR2 was the presence or absence
209 of ChR2 gene expression in SACs. Therefore, it was suggested that photoresponse from
210 SACs enhanced the maintained response of RGCs, enhancing the visual restoration effect
211 via acetylcholine and gap junctions.
212
213 **Induction efficiency into SACs tended to affect visual restoration.**
214 Finally, to investigate its clinical applicability, the effect of SACs on visual restoration was
215 examined using rAAV2, which is already approved for gene therapy [35]. We injected rAAV2-
216 CAG-ChR2-tdimer2 intravitreally into *rd1* mice and performed MEA, VEP, and LDT
217 (Figure 4A, Figure S8A, B). In addition, we counted the number of transfected RGCs and
218 SACs and analyzed their relevance to visual restoration effects. As a result of
219 immunohistochemical labeling using RBPMS, the infection efficiency to RGCs was 24%,
220 which was equivalent to previous reports (21-23%) [10,36,37], and significantly less than those
221 of our transgenic mice (Figure 4B, C). The efficiency to SACs was 12%, which was also

222 less than that of transgenic mice (Figure 4D, E). As a result of MEA recording, the peak
223 response in the rAAV model was equivalent to that of both transgenic lines (Figure S8C),
224 and the maintained response and its rate were equal to that of the M4 line (Figure S8D, E),
225 perhaps because the input from various cell types other than SACs is also included in the
226 rAAV model. This outcome suggests that the increase in the maintained response is not
227 specific to gene transfer in SACs. Each average of the VEP amplitude in the *rd1*;M4-ChR2,
228 *rd1*;5B-ChR2, and rAAV-treated *rd1* mice in response to the light stimulus at 4000 cds/$m^2$
229 was 72.7 μV (n=10), 70.4 μV (n=12) and 32.2 μV (n=12), respectively. These responses
230 were significantly higher than those in *rd1*;tetO-ChR2 mice (19.1 mV; n=8) but smaller than
231 those in the 8-week-old wild-type C57BL/6J mice (155 μV; n=4) (Figure 4F, G). There was
232 no significant difference between *rd1*;5B-ChR2 and *rd1*;M4-ChR2 mice, and the VEPs of
233 rAAV treated *rd1* mice were smaller than those of them (Figure 4F, G). Even in the LDT
234 results, the restoration effect of rAAV-treated *rd1* mice tended to be lower than that of
235 transgenic mice (Figure 4H), perhaps due to its infection efficiency, or the higher maintained
236 response might not lead directly and simply to better visual restoration. In addition, the
237 correlation between the infection efficiency of SACs in each rAAV-treated *rd1* mouse and
238 the visual restoration effect was investigated. The results showed a significant, positive
239 correlation between the number of transfected SACs in the inner nuclear layer (INL) and

240 the maintained to peak ratio in MEA (Figure 4I), a positive correlation between the VEP
241 amplitude (Figure 4J) and a significant, negative correlation between the time spent in the
242 bright half in LDT (Figure 4K). This outcome suggests that the maintained response in MEA
243 is derived from SACs and that, clinically, including not only RGCs but also SACs is more
244 effective for visual restoration. Although there is a limitation because infection efficiency is
245 a confounding factor, there was no correlation between the number of transfected RGCs in
246 GCL and the maintained to peak ratio in MEA (Figure S8F), and the correlation of the
247 number of transfected SACs in the inner nuclear layer (INL) with the VEP amplitude (Figure
248 4J) and the time spent in the bright half in LDT (Figure 4K) was stronger than that with
249 infection efficiency into RGCs (Figure S8G, H).
250

251 **Discussion**

252 In this study, we established transgenic mouse lines inducing gene induction in specific
253 retinal cells using the tet-system (Figure S1). We identified that gene induction occurred in
254 RGCs and SACs under the control of a muscarinic acetylcholine receptor *Chrm4* promoter,
255 whereas a serotonin (5-HT) *Htr5b* receptor control region led to induction only in RGCs in
256 the retina (Figure 2). Among acetylcholine receptors expressed by all types of neurons in
257 the retina [38–43], the *Chrm4* muscarinic receptor is expressed in RGCs and amacrine cells [38,44].

258 All of the amacrine cell expression in the M4 line was consisted of type-a SACs (Figure
259 1M-T, Figure S3 A-L). There are two subytpes of SACs, type-a and type-b (displaced
260 SACs)[45,46]. This would be the first report of a transgenic line specific to only type-a but not
261 type-b SACs.The 5-HT *Htr5b* receptor is expressed in rodents but not in humans [47].
262 Although several types of 5HT receptors are expressed in the mouse retina [48], the retinal
263 distribution of *Htr5b* receptor has not been previously described to our knowledge. We
264 found that these gene inductions in both mouse retinas indicated that these strain are useful
265 for examining the functions of RGCs and SACs.
266
267 Accumulating data have shown that the visual restoration strategy induced by optogenetic
268 genes is a promising therapy for degenerative retinal diseases. Most of the amacrine cells
269 are inhibitory neurons in the vertebrate retina, which have not been regarded much in the
270 elementary visual restoration target. The results of this study showed that SACs increase
271 the maintained response through gap junctions and contribute to enhancing the visual
272 restoration effect. In particular, since the restoration effect of LDT and OKR was more
273 significant than that of VEP, it might contribute to sustained behavior and direction
274 recognition rather than transient response, consistent with the role of the maintained
275 response in RGCs [49]. Including the results using rAAV, in the current situation, viral

276 delivery in primates is limited [31], and gene transfer involving amacrine cells, for example,

277 using ubiquitous promoters, might be more effective in visual restoration than limiting

278 RGCs in the clinical setting.

279

280 **Methods**

281 **Key Resources Table**

| REAGENT or RESOURCE | SOURCE | IDENTIFIER |
|---|---|---|
| Chemicals, Peptides, and Recombinant Proteins | | |
| N-Nitroso-N-methylurea | Toronto Research Chemicals | M325815 |
| Domitor® (medetomidine hydrochloride) | Zenoac | |
| Antisedan® (atipamezole) | Zenoac | |
| Midazolam Sandoz™ | Sandoz | |
| Vetorphal® (butorphanol) | Meiji Seika Pharma | |
| Ames' Medium | Sigma | A1420 |
| L-AP4 | Abcam | ab120002 |
| Meclofenamic acid sodium salt | Sigma | M4531 |
| TPMPA | TOCRIS | 1040 |
| CNQX | Abcam | ab120044 |
| D-AP5 | Abcam | ab120003 |
| Carbenoxolone | MERCK | C4790 |
| Atropine | MERCK | A0132 |
| DAPI | Life Technologies | D21490 |
| Anti-RBPMS antibody | Abcam | ab194213 |
| Anti-Choline Acetyltransferase Antibody | Abcam | ab114p |
| Anti-VGluT2 | Frontier Institute | VGluT2-Rb-Af720 |
| Anti-Syntaxin antibody | Abcam | ab3265 |
| Anti-Tyrosine Hydroxylase antibody | Abcam | ab112 |
| Anti-Prox1 antibody | AngioBio | 11-002P |

| | | |
|---|---|---|
| pAAV CAG ChR2 E123T T159C 2A tDimer | Addgene | #85399 |
| Experimental Models: Organisms/Strains | | |
| Mouse: C3H/HeJJcl | CLEA Japan | |
| Mouse: tetO-YCnano50 | RIKEN BRC | RBRC09550 |
| Mouse: tetO-ChR2 (E123T/T159C) | RIKEN BRC | RBRC05843 |
| Mouse: *Chrm4*-tTA | RIKEN BRC | RBRC09551 |
| Mouse: *Htr5b*-tTA | RIKEN BRC | RBRC05445 |
| Oligonucleotides | | |
| Genotyping primer: tet-Foward: CATGAAGCAGCACGACTTCTT | | |
| Genotyping primer: tet-Reverse: TTCTTACTTGTACAGCTCGTCCA | | |
| Genotyping primer: M4-Foward: AAGCACCAAGTTCTCTCCCGTCTT | | |
| Genotyping primer: M4-Reverse: CGGAGTTGATCACCTTGGACTTGT | | |
| Genotyping primer: 5B-Foward: GCTCCAGGAAACCACAATGCCTTT | | |
| Genotyping primer: 5B-Reverse: CGGAGTTGATCACCTTGGACTTGT | | |
| Genotyping primer: *rd1*-Forward: AAGCTAGCTGCAGTAACGCCATTT | | |
| Genotyping primer: wild-Forward: ACCTGCATGTGAACCCAGTATTCTATC | | |
| Genotyping primer: *rd1* wild common-Reverse: CTACAGCCCCTCTCCAAGGTTTATAG | | |

282

283 **Animals**

284 Transgenic mice used for the experiments and their genotyping protocols were generated as

285 previously reported[14]. Mice homozygous for the retinal degeneration alleles Pde6b$^{rdl}$

286 (C3H/HeJJcl, *rd1*) and WT C57BL/6J were obtained from CLEA Japan, Inc. Animals were
287 maintained under 12-h light:12-h-dark conditions. For animals bred in house, littermates of
288 the same sex were randomized to experimental groups. Mice used for the experiments were
289 heterozygous for the tTA and tetO genes and homozygous for the *rd1* gene. All of the animal
290 experiments were conducted in accordance with protocols approved by Institutional Animal
291 Care and Use Committee of Keio University School of Medicine.
292 tetO-YC (RBRC09550), tetO-ChR2 (RBRC05843), *Chrm4*-tTA (RBRC09551), and *Htr5b*-
293 tTA (RBRC05445) are available from RIKEN Bioresource Center in Japan.
294 Study approval: All of the animal experiments were conducted in accordance with protocols
295 approved by Institutional Animal Care and Use Committee of Keio University School of
296 Medicine (#2808).
297
298 **Immunohistochemistry**
299 The protocol for immunohistochemistry was previously described. The retinas were
300 incubated in PBS with 1% Triton X-100 and 0.5% Tween 20 for 1 h at room temperature
301 and in 4% BSA for 1 h at room temperature and then incubated overnight at 4 ˚C with
302 primary antibodies: RBPMS (1:500, Abcam, Cambridge, UK), ChAT (1:100, Abcam),
303 VGLUT2 (1:100, Frontier Institute, Hokkaido, Japan), syntaxin (1:100, Abcam), tyrosine

304 hydroxylase (1:100, Abcam) and Prox1 (1:100, AngioBio, San Diego, CA, USA) in
305 blocking buffer. Secondary anti-rabbit, mouse and goat IgG, conjugated with Alexa TM488,
306 TM594 and 633, respectively (1:1000; Molecular Probes), were applied for 1 h at room
307 temperature. The retinas then were flat mounted, and the sections were mounted on slide
308 glass.
309

310 **Vector production and purification**

311 pAAV-CAG–ChR2(E123T/T159C)-tdimer2–WPRE (Addgene, Watertown, MA) was used.
312 Type 2 serotypes of rAAV vectors were prepared using the AAV Helper Free Packaging
313 System (Cell Biolabs, San Diego, CA, USA). The serotypes were produced in HEK 293
314 cells using a helper virus-free system and were purified using two $CsCl_2$ density gradients
315 and titrated by quantitative polymerase chain reaction. Final preparations were dialyzed
316 against phosphate-buffered saline (PBS) and stored at -80°C.
317

318 **Virus injection**

319 The mice were anesthetized with a combination of midazolam, medetomidine and
320 butorphanol tartrate at doses of 4 mg/kg, 0.75 mg/kg and 5 mg/kg of body weight and placed
321 on a heating pad that maintained their body temperatures at 35–36°C throughout the

322 experiments. An aperture was made next to the limbus through the sclera with a 30-gauge
323 disposable needle, and a 33-gauge unbeveled blunt-tip needle on a Hamilton syringe was
324 introduced through the scleral opening into the vitreous space for intravitreal injections and
325 introduced through the scleral opening along the scleral interior wall into the subretinal
326 space for subretinal injections. Each eye received 1 μl of vehicle (PBS) or vector at a titer
327 of $2.0 \times 10^{11}$ vg/ml.
328
329 **Multielectrode array recordings**
330 All of the procedures were performed under dim red light. The mice were anesthetized and
331 euthanized by quick cervical dislocation. Following enucleation, the retina was dissected at
332 room temperature in Ames' medium bubbled with 95% O2/5% CO2 (A 1420; Sigma-
333 Aldrich). The separated retina was placed on a cellulose membrane, and RGC was directed
334 to the electrode and was gently contacted against MEA (MEA2100-Systems; Multi Channel
335 Systems, Reutlingen, Germany) under suction pressure. During the experiment, the retinas
336 were continuously perfused with Ames' medium bubbling at 34 ° C. at a rate of 1-2 ml/min.
337 Recorded signals were collected, amplified, and digitized using MC Rack software (Multi
338 Channel Systems). Retinas were perfused for 30 min in darkness before recording responses.
339 A 470-nm blue LED light at $1.0 \times 10^{16}$ photons·$cm^{-2}$·$s^{-1}$ stimulus was used. L-(+)-2-amino-

340 4-phosphonobutyric acid (L-AP4, ab120002; Abcam), (1,2,5,6-tetrahydropyridin-4-yl)
341 methylphosphinic acid (TPMPA, Cat. No. 1040; Tocris Bio-Science), meclofenamic acid
342 sodium salt (MFA, M4531; Sigma-Aldrich), atropine (A0132; MERCK) and carbenoxolone
343 (C4790; MERCK) were newly diluted to 20 μM, 20 μM, 100 μM, 20 μM and 100 μM
344 respectively. Stimulation was presented for 1 seconds at 60-second intervals. Signals were
345 filtered between 200 Hz (low cutoff) and 20 kHz (high cutoff). A threshold of 40 μV was
346 used to detect action potentials, and action potentials from individual neurons were
347 determined via a standard expectation–maximization algorithm using Off-line Sorter
348 software (Plexon, Dallas, TX, USA). The results were plotted using NeuroExplorer software
349 (Nex Technologies Colorado Springs, CO, USA). Maintained-to-peak amplitude ratio was
350 calculated by dividing the maintained response amplitude in maintaining time frame (0.4 to
351 1.0 seconds after light stimulation) by the peak amplitude (this ratio quantifies the
352 sustenance of the response).
353
354 **ERG analyses**
355 Scotopic ERGs were recorded according to a previous report [50]. Animals were dark-adapted
356 for 12 h and prepared under dim red illumination. The mice were anesthetized with a
357 combination of midazolam, medetomidine and butorphanol tartrate at doses of 4 mg/kg,

358 0.75 mg/kg and 5 mg/kg of body weight, respectively and were placed on a heating pad that
359 maintained their body temperature at 35–36°C throughout the experiments. The pupils were
360 dilated with a mixed solution of 0.5% tropicamide and 0.5% phenylephrine (Mydrin-P;
361 Santen, Osaka, Japan). The ground electrode was a subcutaneous needle in the tail, and the
362 reference electrode was placed subcutaneously between the eyes. The active contact lens
363 electrodes (Mayo, Inazawa, Japan) were placed on the corneas. Recordings were performed
364 with a PuREC acquisition system (Mayo). Responses were filtered through a bandpass filter
365 ranging from 0.3 to 500 Hz to yield a- and b-waves. White LED light stimulations of 10.0
366 log cd-s/$m^2$ were delivered via a Hemisphere LS-100 Stimulator (Mayo).
367
368 **VEP analyses**
369 The measuring electrodes were placed more than one week before the measurement. The
370 mice were anesthetized with a combination of midazolam, medetomidine and butorphanol
371 tartrate at doses of 4 mg/kg, 0.75 mg/kg and 5 mg/kg of body weight, respectively. The
372 animals were placed in a stereotaxic holder. A stainless-steel screw (M1.0×6.0 mm) inserted
373 through the skull into the both visual cortex (1.5 mm laterally to the midline, 1.5 mm anterior
374 to the lambda), penetrating the cortex to approximately 1 mm, served as a measuring
375 electrode.

376 At the time of the measurement, the mice were anesthetized again with the same doses.
377 Visual stimuli were generated by a white LED placed 3 cm from the eye. It was stimulated
378 with 100-ms pulses of white LED 4000 cds/m$^2$ light stimulus intensity. Signals were
379 acquired and analyzed with a PuREC acquisition system (Mayo). Signals were low-pass
380 filtered at 300 Hz and averaged over the 60 trials.
381

382 **OKR recording system**

383 Protocols for eye movement recording and visual stimulation were previously described [51,52].
384 Eye movements were recorded from both eyes of each animal separately. During the
385 recording, the contralateral eye was covered by aluminum foil. The head of the mouse was
386 fixed to an experimental steel board by the head-mounted stick for the LIM lens frames.
387 The reflected images through a hot mirror (43957-J, Edmund) were recorded using an
388 infrared CCD camera (BS-GV200, Libraly Inc., Tokyo, Japan). The images of the eye
389 movements were processed and analyzed using software (Move-tr/2D, Libraly Inc., Tokyo,
390 Japan). The sampling rate of the image was 200 Hz. The center of the pupil was detected by
391 software. We calculated the speed of the eye movements on two-dimensional images and
392 converted them to angular speeds using the AL of each eye. The spatial frequency was set
393 as 0.125 cycles/degree, and the temporal frequency of the visual stimulus was 1.5 Hz. The

394 motion onset delay (MOD) was set as 333 msec. Continuing the MOD, sinusoidal grating
395 started to move clockwise in 5 sec. The intervals of visual stimulus were 60 sec. Eye
396 movements were recorded three times for each experiment to exclude shaking images due
397 to excessive body movements. Average velocities of the eye movements were calculated in
398 the slow speed phase of their nystagmus.
399
400 **LDT recording**
401 Mice were tested in a 30 × 45 × 30-cm box, containing equally sized light and dark chambers
402 connected by a 5 × 5-cm opening via which mice could move freely. The bright half of the
403 box was illuminated from above by a white fluorescent light with intensity of 200 lux
404 measured at the floor level. The animals were placed in the bright half and movement
405 recorded (HD Pro Webcam C920, Logitech, Lausanne, Switzerland). A trial lasted 10 min,
406 and then the testing apparatus was dismantled and cleaned with 70% ethanol. Videos were
407 analyzed using ANY-maze tracking software and were validated by comparison with
408 manual analysis. Time spent in the bright half was recorded.
409
410 **Preparation of whole-mount samples and cryosections of retinas**

411 Enucleated eyes were fixed for 20 min in 4% paraformaldehyde (PFA) in PBS and then
412 dissected as previously described [53]. The obtained tissues were post-fixed overnight in 4%
413 PFA in PBS and stored in methanol at –20°C. Cryosections of retinas (12 mm) were
414 prepared as previously described [54], after the eyeballs were immersed overnight in 4% PFA.
415 Retinal sections were observed using a confocal microscope (LSM710; Carl Zeiss, Jena,
416 Germany).
417
418 **OCT Imaging**
419 The thickness of the retina was analyzed by an SD-OCT system (Envisu R4310; Leica,
420 Wetzlar, Germany) tuned for mice. The imaging protocol entailed a 3 mm×3 mm perimeter
421 square scan sequence producing a single en-face image of the retina through a 50-degrees
422 field of view from the mouse lens, following mydriasis. The en-face image consisted of 100
423 B-scan tomograms with each B-scan consisting of 1000 A-scans. The retinal thickness of
424 150 μm from the optic disc of each quadrant was measured.
425
426 **Quantification and Statistical Analysis**

All of the results are expressed as the mean ± SEM. The averaged variables were compared using the Student's 2-tailed t-test and the Kruskal Wallis one-way ANOVA test. P-values of less than 0.05 were considered statistically significant.

**Data and Software Availability**

Raw MEA spike data were sorted offline to identify single units using Offline Sorter software (version 4.4.0)(Plexon). Spike-sorted data were analyzed with NeuroExplorer 5 software (version 5.115) (Nex Technologies).

## Author Contribution

Y.K. and T.K. designed the research, wrote the manuscript, and performed the retinal histology, MEA, ERG and VEP recordings, and LDT experiments. K.K. performed AAV production. Y.K. and H.K. performed OKR recording. Y.K. performed data processing and analysis. H.O and T.K. made critical revisions of the manuscript. T.K. supervised the research.


## Acknowledgements

We would like to thank Prof. Amane Koizumi for critical comments to the manuscript. Y.K. is supported by grants from the Keio University Doctorate Student Grant-in-Aid Program. T.K. is supported by Grants-in-Aid from Takeda Science Foundation and the Keio University Medical Science Fund.


## Declaration of Interests

The authors declare no competing interests.

452 **References**


453 1. Sahel, J.-A., Marazova, K. & Audo, I. Clinical characteristics and current
454 therapies for inherited retinal degenerations. *Cold Spring Harb. Perspect. Med.* **5**,
455 a017111 (2014).

456 2. Bi, A. *et al.* Ectopic Expression of a Microbial-Type Rhodopsin Restores Visual
457 Responses in Mice with Photoreceptor Degeneration. *Neuron* **50**, 23–33 (2006).

458 3. Doroudchi, M. M. *et al.* Virally delivered Channelrhodopsin-2 Safely and
459 Effectively Restores Visual Function in Multiple Mouse Models of Blindness.
460 *Mol. Ther.* **19**, 1220–1229 (2011).

461 4. Lagali, P. S. *et al.* Light-activated channels targeted to ON bipolar cells restore
462 visual function in retinal degeneration. *Nat. Neurosci.* **11**, 667–675 (2008).

463 5. Cronin, T. *et al.* Efficient transduction and optogenetic stimulation of retinal
464 bipolar cells by a synthetic adeno-associated virus capsid and promoter. *EMBO*
465 *Mol. Med.* **6**, 1175–90 (2014).

466 6. Macé, E. *et al.* Targeting channelrhodopsin-2 to ON-bipolar cells with vitreally
467 administered AAV restores ON and OFF visual responses in blind mice. *Mol.*
468 *Ther.* **23**, 7–16 (2014).

469 7. Busskamp, V. *et al.* Genetic reactivation of cone photoreceptors restores visual

470 responses in retinitis pigmentosa. *Science* **329**, 413–7 (2010).

471 8. Van Wyk, M., Pielecka-Fortuna, J., Löwel, S. & Kleinlogel, S. Restoring the ON
472 Switch in Blind Retinas: Opto-mGluR6, a Next-Generation, Cell- Tailored
473 Optogenetic Tool. *PLoS Biol* **13**, (2015).

474 9. Pienaar, A., Bedford, R., Davis, K. & Bishop, P. N. Restoration of vision with
475 ectopic expression of human rod opsin. *Curr. Biol.* **25**, 1–35 (2015).

476 10. Bi, A. *et al.* Ectopic Expression of a Microbial-Type Rhodopsin Restores Visual
477 Responses in Mice with Photoreceptor Degeneration. *Neuron* **50**, 23–33 (2006).

478 11. Lagali, P. S. *et al.* Light-activated channels targeted to ON bipolar cells restore
479 visual function in retinal degeneration. *Nat. Neurosci.* **11**, 667–675 (2008).

480 12. Lin, J. Y., Lin, M. Z., Steinbach, P. & Tsien, R. Y. Characterization of
481 Engineered Channelrhodopsin Variants with Improved Properties and Kinetics.
482 *Biophys. J.* **96**, 1803–1814 (2009).

483 13. Gossen, M. *et al.* Transcriptional activation by tetracyclines in mammalian cells.
484 *Science* **268**, 1766–9 (1995).

485 14. Tanaka, K. F. *et al.* Expanding the repertoire of optogenetically targeted cells
486 with an enhanced gene expression system. *Cell Rep.* **2**, 397–406 (2012).

487 15. Takata, N. *et al.* Optogenetic astrocyte activation evokes BOLD fMRI response

488 with oxygen consumption without neuronal activity modulation. *Glia* **66**, 2013–
489 2023 (2018).
490 16. Kanemaru, K. *et al.* In Vivo visualization of subtle, transient, and local activity of
491 astrocytes using an ultrasensitive Ca2+ indicator. *Cell Rep.* **8**, 311–318 (2014).
492 17. Rodriguez, A. R., de Sevilla Müller, L. P. & Brecha, N. C. The RNA binding
493 protein RBPMS is a selective marker of ganglion cells in the mammalian retina.
494 *J. Comp. Neurol.* **522**, 1411–43 (2014).
495 18. Tsunematsu, T. *et al.* Optogenetic manipulation of activity and temporally
496 controlled cell-specific ablation reveal a role for MCH neurons in sleep/wake
497 regulation. *J. Neurosci.* **34**, 6896–6909 (2014).
498 19. Tsubura, A., Yoshizawa, K., Kuwata, M. & Uehara, N. Animal models for
499 retinitis pigmentosa induced by MNU ; disease progression , mechanisms and
500 therapeutic trials Histology and. 933–944 (2010).
501 20. Vaney, D. I., Sivyer, B. & Taylor, W. R. Direction selectivity in the retina:
502 Symmetry and asymmetry in structure and function. *Nat. Rev. Neurosci.* **13**, 194–
503 208 (2012).
504 21. Bi, A. *et al.* Ectopic expression of a microbial-type rhodopsin restores visual
505 responses in mice with photoreceptor degeneration. *Neuron* **50**, 23–33 (2006).

506 22. Yoshida, K. *et al.* A key role of starburst amacrine cells in originating retinal
507 directional selectivity and optokinetic eye movement. *Neuron* **30**, 771–80 (2001).
508 23. Carter-Dawson, L. D., LaVail, M. M. & Sidman, R. L. Differential effect of the
509 rd mutation on rods and cones in the mouse retina. *Invest. Ophthalmol. Vis. Sci.*
510 **17**, 489–98 (1978).
511 24. Association for Research in Vision and Ophthalmology., L. D., LaVail, M. M. &
512 Sidman, R. L. *Investigative ophthalmology & visual science. Investigative*
513 *Ophthalmology & Visual Science* **17**, (C.V. Mosby Co, 1977).
514 25. Taylor, W. R. & Smith, R. G. The role of starburst amacrine cells in visual signal
515 processing. *Vis. Neurosci.* **29**, 73–81 (2012).
516 26. Yamada, E. S. *et al.* Synaptic connections of starburst amacrine cells and
517 localization of acetylcholine receptors in primate retinas. *J. Comp. Neurol.* **461**,
518 76–90 (2003).
519 27. Yonehara, K. *et al.* Spatially asymmetric reorganization of inhibition establishes
520 a motion-sensitive circuit. *Nature* **469**, 407–410 (2011).
521 28. Marc, R. E. *et al.* Heterocellular coupling between amacrine cells and ganglion
522 cells. *Front. Neural Circuits* **12**, 1–23 (2018).
523 29. Völgyl, B., Chheda, S. & Bloomfield, S. A. Tracer coupling patterns of the

524 ganglion cell subtypes in the mouse retina. *J. Comp. Neurol.* **512**, 664–687
525 (2009).
526 30. Bloomfield, S. A. & Volgyi, B. The diverse functional roles and regulation of
527 neuronal gap junctions in the retina. *Nat Rev Neurosci* **10**, 495–506 (2009).
528 31. Sengupta, A. *et al.* Red-shifted channelrhodopsin stimulation restores light
529 responses in blind mice , macaque retina , and human retina. *EMBO Mol Med* 1–
530 17 (2016). doi:10.15252/emmm.201505699
531 32. Pan, Z. H., Ganjawala, T. H., Lu, Q., Ivanova, E. & Zhang, Z. ChR2 mutants at
532 L132 and T159 with improved operational light sensitivity for vision restoration.
533 *PLoS One* (2014). doi:10.1371/journal.pone.0098924
534 33. Wu, C., Ivanova, E., Zhang, Y. & Pan, Z.-H. rAAV-Mediated Subcellular
535 Targeting of Optogenetic Tools in Retinal Ganglion Cells In Vivo. *PLoS One* **8**,
536 e66332 (2013).
537 34. Mure, L. S. *et al.* Melanopsin-Encoded Response Properties of Intrinsically
538 Photosensitive Retinal Ganglion Cells. *Neuron* **90**, 1–12 (2016).
539 35. Keeler, A. M. & Flotte, T. R. Recombinant Adeno-Associated Virus Gene
540 Therapy in Light of Luxturna (and Zolgensma and Glybera): Where Are We, and
541 How Did We Get Here? *Annu. Rev. Virol.* **6**, 601–621 (2019).

542 36. Chaffiol, A. *et al.* A New Promoter Allows Optogenetic Vision Restoration with
543 Enhanced Sensitivity in Macaque Retina. *Mol. Ther.* **25**, 2546–2560 (2017).
544 37. Lin, B., Koizumi, A., Tanaka, N., Panda, S. & Masland, R. H. Restoration of
545 visual function in retinal degeneration mice by ectopic expression of melanopsin.
546 *Proc. Natl. Acad. Sci. U. S. A.* **105**, 16009–16014 (2008).
547 38. Strang, C. E., Renna, J. M., Amthor, F. R. & Keyser, K. T. Muscarinic
548 Acetylcholine Receptor Localization and Activation Effects on Ganglion
549 Response Properties. *Investig. Opthalmology Vis. Sci.* **51**, 2778 (2010).
550 39. Keyser, K. T. *et al.* Amacrine, ganglion, and displaced amacrine cells in the
551 rabbit retina express nicotinic acetylcholine receptors. *Vis. Neurosci.* **17**, 743–52
552 40. Dmitrieva, N. A., Strang, C. E. & Keyser, K. T. Expression of Alpha 7 Nicotinic
553 Acetylcholine Receptors by Bipolar, Amacrine, and Ganglion Cells of the Rabbit
554 Retina. *J. Histochem. Cytochem.* **55**, 461–476 (2007).
555 41. Liu, J. *et al.* Nicotinic Acetylcholine Receptor Subunits in Rhesus Monkey
556 Retina. *Investig. Opthalmology Vis. Sci.* **50**, 1408 (2009).
557 42. Blute, T. A., Strang, C., Keyser, K. T. & Eldred, W. D. Activation of the
558 cGMP/nitric oxide signal transduction system by nicotine in the retina. *Vis.*
559 *Neurosci.* **20**, 165–76

560 43. Cimini, B. A., Strang, C. E., Wotring, V. E., Keyser, K. T. & Eldred, W. D. Role
561 of acetylcholine in nitric oxide production in the salamander retina. *J. Comp.*
562 *Neurol.* **507**, 1952–1963 (2008).
563 44. Strang, C. E., Long, Y., Gavrikov, K. E., Amthor, F. R. & Keyser, K. T.
564 Nicotinic and muscarinic acetylcholine receptors shape ganglion cell response
565 properties. *J. Neurophysiol.* **113**, 203–217 (2015).
566 45. Famiglietti, E. V. J. 'Starburst' amacrine cells and cholinergic neurons: mirror-
567 symmetric on and off amacrine cells of rabbit retina. *Brain Res.* **261**, 138–144
568 (1983).
569 46. Famiglietti, E. V. Starburst amacrine cells: Morphological constancy and
570 systematic variation in the anisotropic field of rabbit retinal neurons. *J. Neurosci.*
571 **5**, 562–577 (1985).
572 47. Grailhe, R., Grabtree, G. W. & Hen, R. Human 5-HT5 receptors: the 5-HT5A
573 receptor is functional but the 5-HT5B receptor was lost during mammalian
574 evolution. *Eur. J. Pharmacol.* **418**, 157–167 (2001).
575 48. Chen, Y. *et al.* Systems pharmacology identifies drug targets for Stargardt
576 disease–associated retinal degeneration. *J. Clin. Invest.* **123**, 5119–5134 (2013).
577 49. Ikeda, H. & Wright, M. J. Receptive field organization of 'sustained' and

578 'transient' retinal ganglion cells which subserve different functional roles. *J.*
579 *Physiol.* **227**, 769–800 (1972).
580 50. Katada, Y., Kobayashi, K., Tsubota, K. & Kurihara, T. Evaluation of AAV-DJ
581 vector for retinal gene therapy. *PeerJ*
582 51. Tabata, H., Shimizu, N., Wada, Y., Miura, K. & Kawano, K. Initiation of the
583 optokinetic response (OKR) in mice. *J. Vis.* **10**, 13–13 (2010).
584 52. Jiang, X. *et al.* A highly efficient murine model of experimental myopia. *Sci.*
585 *Rep.* **8**, 2026 (2018).
586 53. Kubota, Y., Hirashima, M., Kishi, K., Stewart, C. L. & Suda, T. Leukemia
587 inhibitory factor regulates microvessel density by modulating oxygen-dependent
588 VEGF expression in mice. *J. Clin. Invest.* **118**, 2393–403 (2008).
589 54. Kurihara, T. *et al.* Neuroprotective effects of angiotensin II type 1 receptor
590 (AT1R) blocker, telmisartan, via modulating AT1R and AT2R signaling in
591 retinal inflammation. *Invest. Ophthalmol. Vis. Sci.* **47**, 5545–52 (2006).
592
593

## Figures

### Figure 1. Gene induction of RGCs and SACs in M4-YC and RGCs in 5B-YC

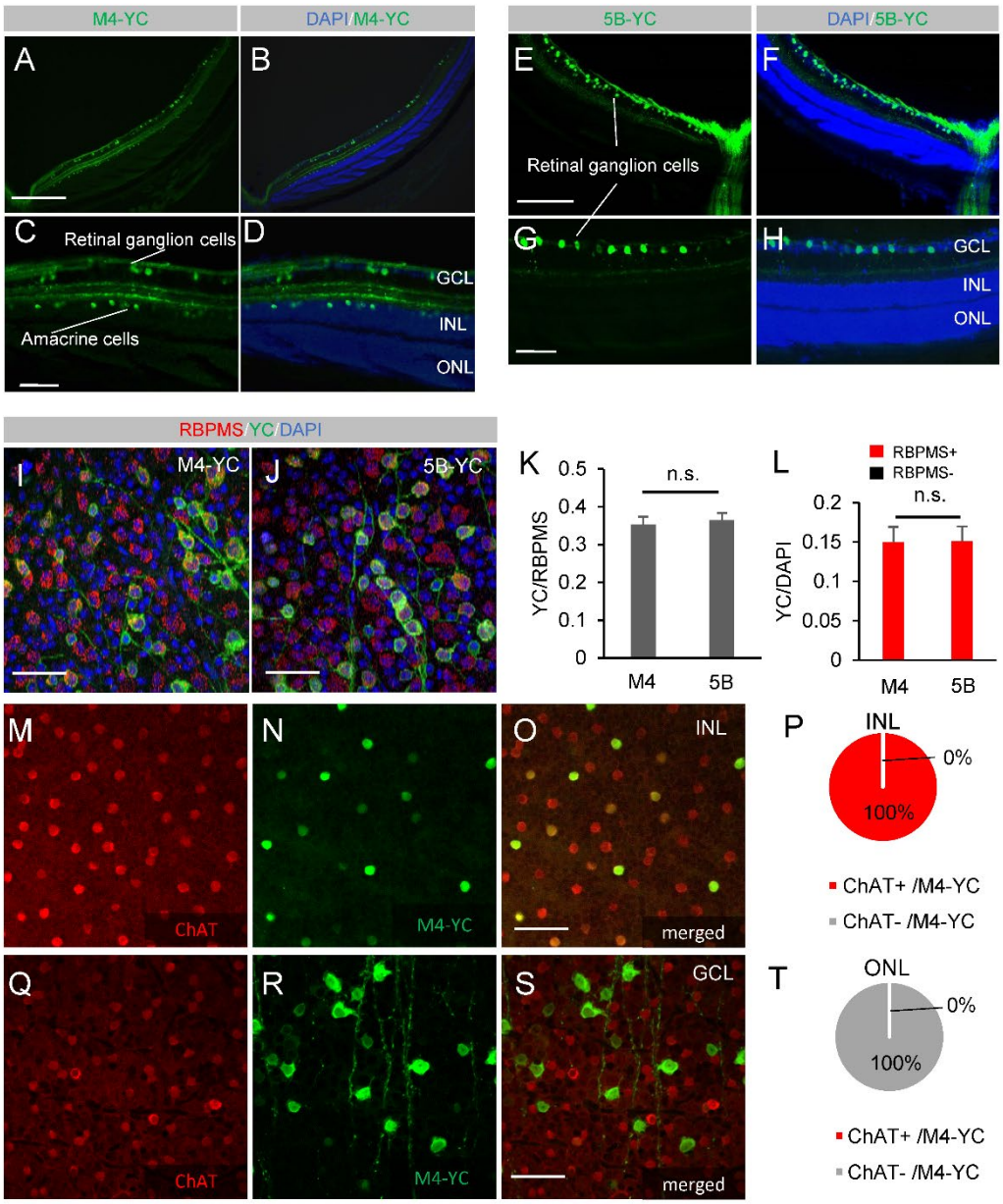

597 In the M4-YC mouse retina, we identified the expression of YC (green) in RGCs and
598 amacrine cells within sections (A-D). In the 5B-YC mouse retina, we identified the
599 expression of YC (green) in RGCs in sections (E-H). Coexpression of the RGC marker
600 RBPMS in flat mounted retinas of M4-YC(I) and 5B-YC(J). Percentage of YC-positive
601 cells in RBPMS-positive (K) or DAPI-positive cells (L) and RBPMS-positive cells in YC-
602 positive cells (L) in both lines from confocal flat mounted GCL (n = 3 retinas each). Regions
603 were chosen in each quadrant, and we obtained RBPMS, DAPI-positive, YC-positive, and
604 co-labeled cells. Coexpression of the starburst amacrine cell marker ChAT in flat mounted
605 retinas of M4-YC in INL (M-O) and GCL (Q-S). Percentage of ChAT-positive cells in YC-
606 positive cells in M4-YC mice from INL (P) and GCL (R) (n = 3 retinas each). Error bars
607 represent the SEMs. INL, inner nuclear layer; GCL, ganglion cell layer, ONL, outer nuclear
608 layer.

609 Scale bar: 50 μm in (E). 100 μm in (B-D), (H), (I), (K), (M), (Q) and (R). 400 μm in (N).
610 500 μm in (F), (G), (O) and (P).

611

**Figure 2. M4-ChR2 mouse shows higher visual restoration effect.**

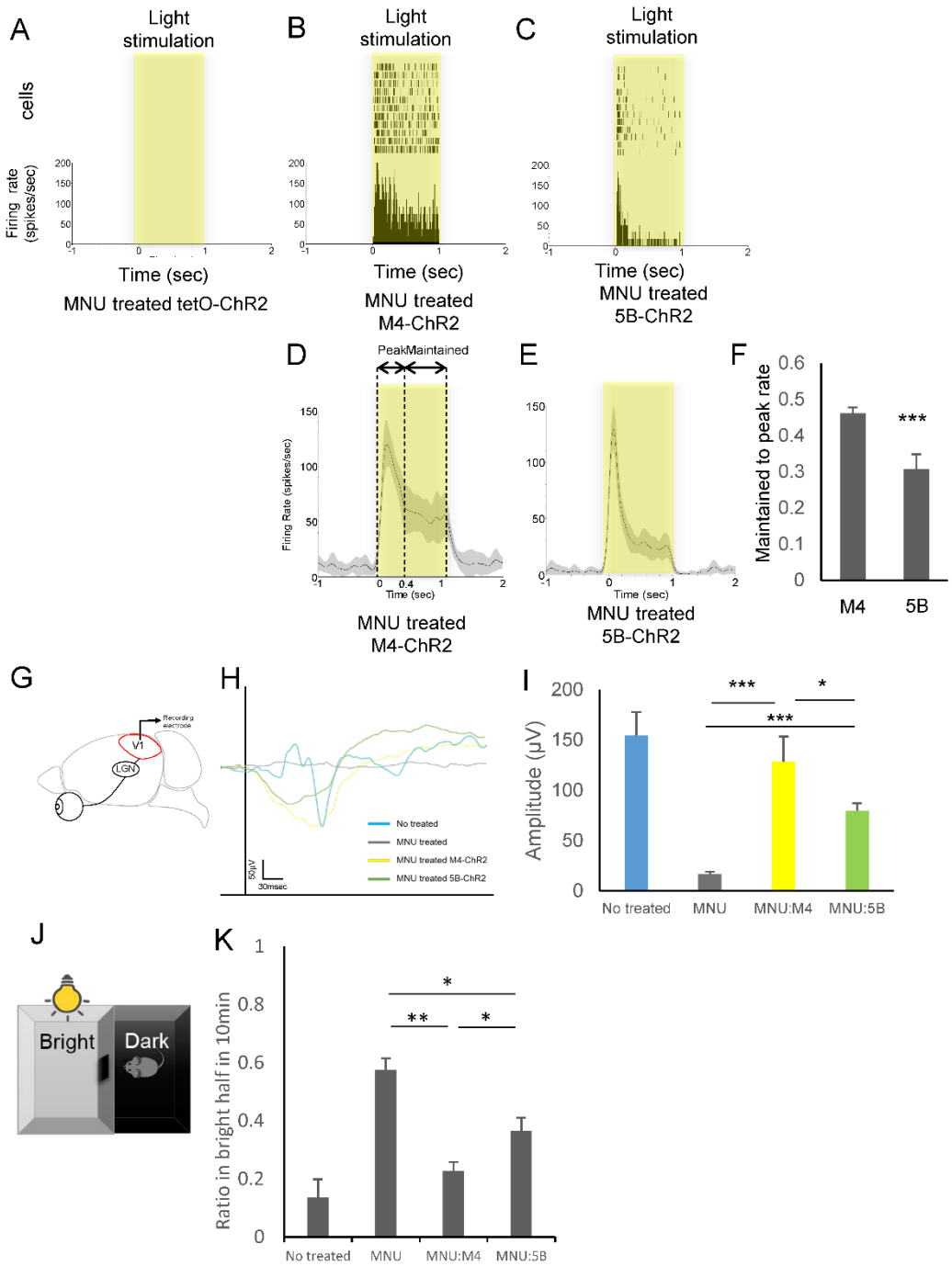

614 (A-C) Raster plots and peri-stimulus time histogram (PSTH) of light stimulation from
615 MNU-treated tetO-ChR, M4-ChR2 and 5B-ChR2 mice. Light intensity was 13.6 log
616 photons/cm$^2$/s, and the duration was 1.0 second. (D, E) The averaged rate histogram after
617 filtering with the Gaussian function from M4-ChR2 and 5B-ChR2 mice. The gray areas
618 around the averaged traces represent the SEM. (F) Maintained-to-peak ratio of the spiking
619 responses recorded. Maintained time frame is 0.4 to 1.0 seconds from light stimulation as
620 shown in H (n = 7 retinas, 164 cells in MNU-treated M4-ChR2 mice, and n = 4 retinas, 127
621 cells in MNU-treated 5B-ChR2 mice). Error bars represent SEMs. ***$p < 0.001$. Student's
622 2-tailed t-test. (G) Schematic image of VEP measurement. (H) Representative VEP traces
623 from MNU-injected and control mice. (I) The average amplitude of the VEPs in the control
624 tetO-ChR mice (n = 4), MNU-treated tetO-ChR mice (n = 8), M4-ChR2 mice (n = 14), and
625 5B-ChR2 mice (n = 12) at 10 weeks of age. It was stimulated with 100-ms pulses of white
626 LED 4,000 cds/m$^2$ light stimulus intensity. Signals were low-pass filtered at 300 Hz and
627 averaged over the 60 trials. (J) Schematic image of the LDT. Mice were tested in a 30 × 45
628 × 30-cm box, containing equally sized bright (200 lx at ground level) and dark chambers
629 connected by a 5 × 5-cm opening via, across which the mice could move freely. Visible
630 mice feel uneasy in bright places, so staying time in the bright half gets shorter. (K) % time
631 in bright half at 10 min of control (tetO-ChR2 mice) (n = 4), MNU-injected tetO-ChR2 mice

632 (n = 8), MNU injected M4-ChR2 mice (n = 15), and MNU-injected 5B-ChR2 mice (n = 8)

633 measured from LDT. All error bars represent the SEMs. *$p < 0.05$, **$p < 0.01$, ***$p < 0.001$.

634 One-way ANOVA testing.

**Figure 3. Acetylcholine and gap junctions were involved in the maintained response.**

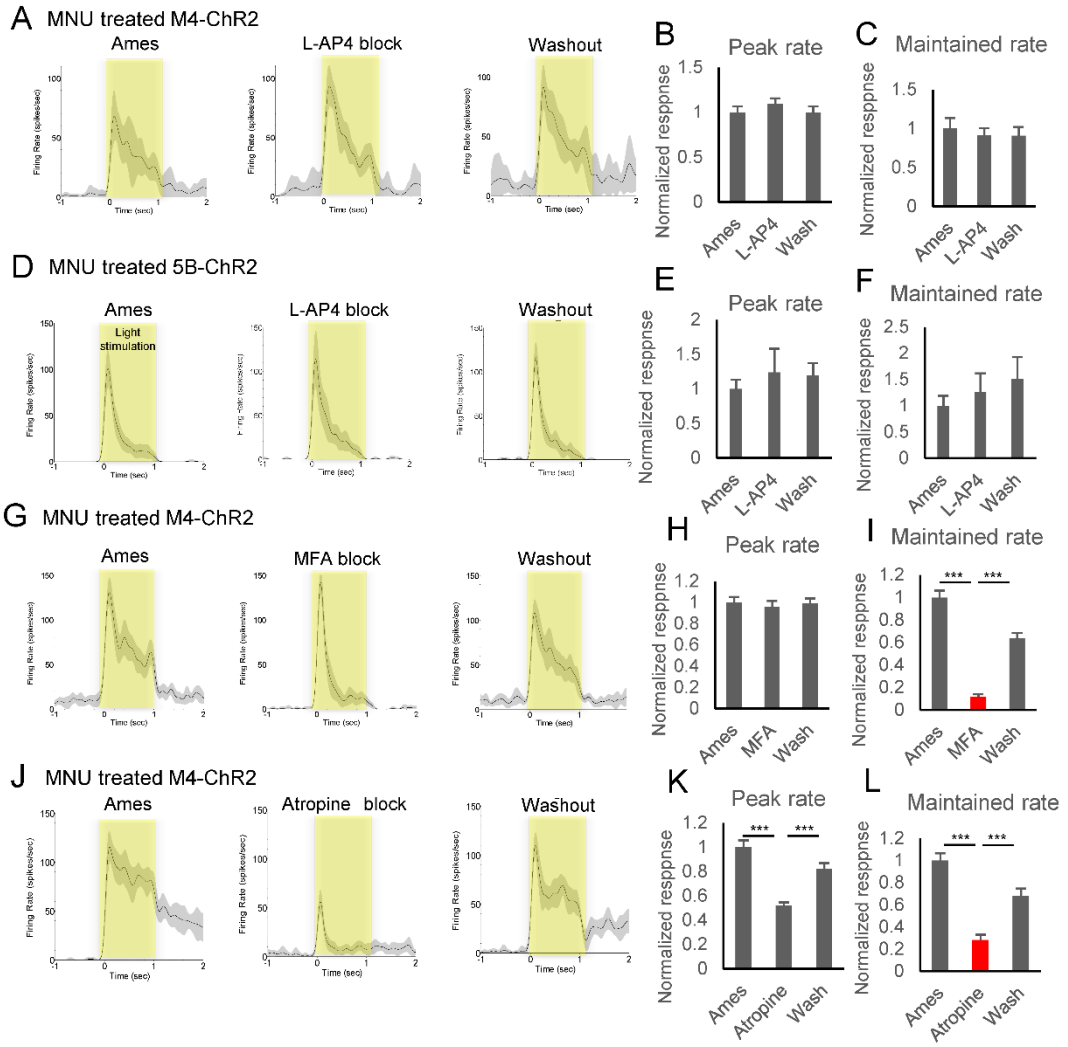


(A, D, G, J) Mean ± SEM of exemplar cell response firing rate recorded during normal Ames' medium superfusion (left), in synaptic block (middle), and after washout (right). MNU-treated M4-ChR2 mice with L-AP4 block (n = 3 retinas, 47 cells) (A), MNU-treated 5B-ChR2 mice with L-AP4 block (n = 3 retinas, 45 cells) (D), MNU-treated M4-ChR2 mice with MFA block (n = 3 retinas, 85 cells) (G), MNU-treated M4-ChR2 mice with atropine

642 block (n = 3 retinas, 33 cells) (J). The gray areas around the averaged traces represent the

643 SEM. (B, C, E, F, H, I, K, L) Averaged normalized peak firing rate and maintained rate.

644 Maintained time frame is 0.4 to 1.0 seconds from light stimulation. Light intensity was 13.6

645 log photons/$cm^2$/s.

646 All error bars represent the SEM. ***$p < 0.001$. One-way ANOVA and Tukey's test.

647

648 **Figure 4. Induction efficiency into SACs tended to affect visual restoration.**

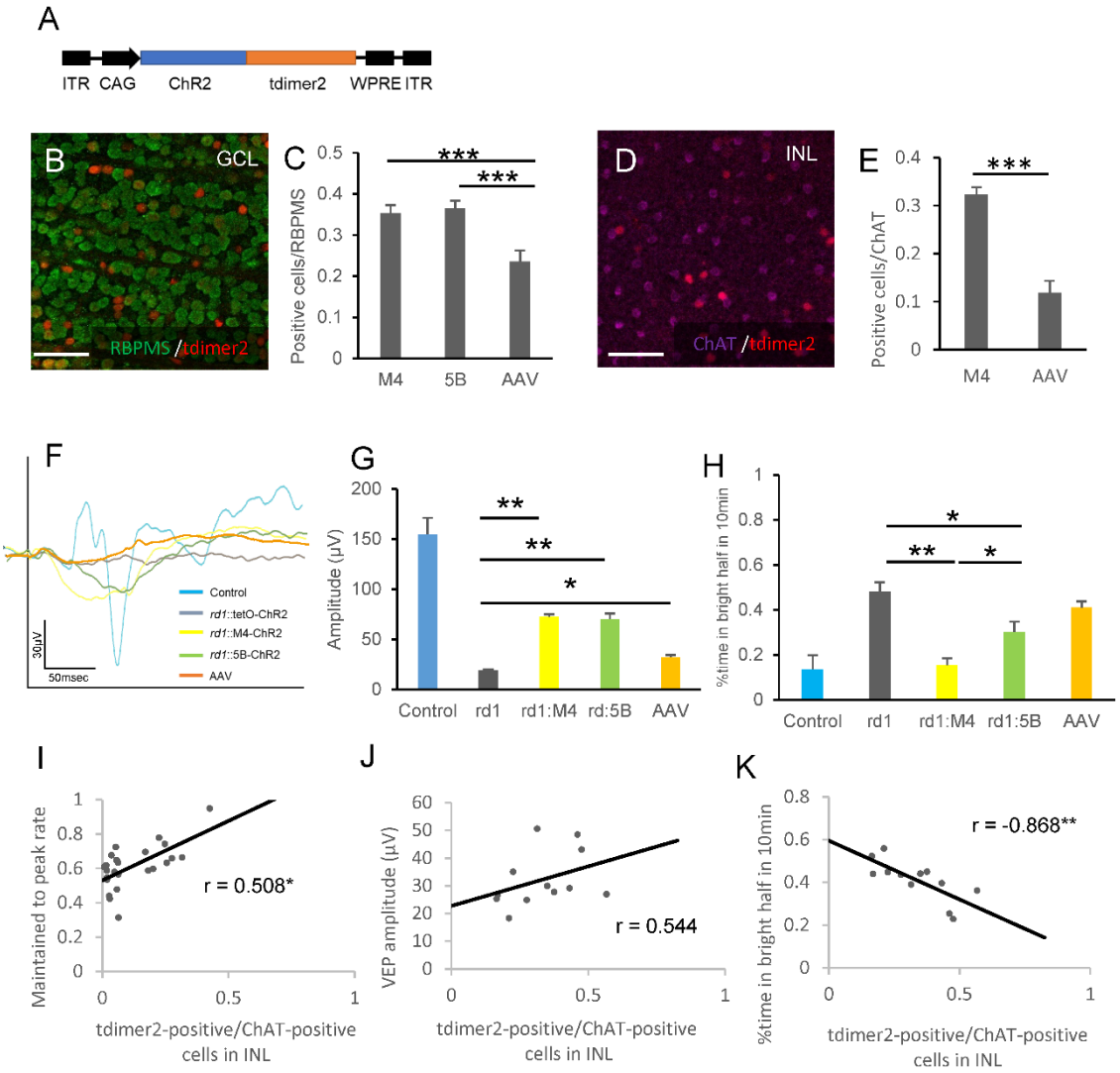


649

650 (A) The rAAV2–CAG-ChR2–tdimer2–WPRE expression cassette: ITR, inverted

651 terminal repeat; WPRE, woodchuck hepatitis virus posttranscriptional regulatory

652 element. (B-E) Coexpression of the RGC marker RBPMS (B) and starburst amacrine

653 cell marker ChAT (D) and tdimer2 in flat mounted retinas of rAAV2–CAG–tdimer2–

654 WPRE treated retinas in *rd1* mice. (C, E) Percentage of YC-positive cells in M4-YC
655 and 5B-YC mice and tdimer2-positive cells in rAAV-treated mice in RBPMS-positive
656 (C) or ChAT-positive cells (E) from confocal flat mounted retina (n = 3 retinas each).
657 Regions were chosen in each quadrant, and we obtained RBPMS, ChAT-positive,
658 YC/tdimer2-positive, and co-labeled cells. (F, G) Average VEP traces (F) and
659 quantification of its amplitudes (G) from control (tetO-ChR2) (n = 3), *rd1*::tetO-ChR2
660 (n = 6), *rd1*;M4-ChR2 (n = 12), *rd1*;5B-ChR2 (n = 12) and rAAV treated *rd1*::tetO-
661 ChR2 mice (n = 12) at 10 weeks of age. It was stimulated with 100-ms pulses of white
662 LED 4,000 cds/m$^2$ light stimulus intensity. Signals were low-pass filtered at 300 Hz and
663 averaged over the 60 trials. (H) % time in bright half at 10 min in control (tetO-ChR2)
664 (n = 3), *rd1*::tetO-ChR2 (n = 6), *rd1*;M4-ChR2 (n = 12), *rd1*;5B-ChR2 (n = 12) and
665 rAAV-treated *rd1*::tetO-ChR2 mice (n = 12) measured from LDT. (I-K) Correlation
666 between transfection efficiency into SACs (tdimer2-positive cells/ChAT-positive cells
667 in INL) and maintained to peak rate (I) (n = 24), VEP amplitude (J) (n = 24) and % time
668 in bright half in LDT (K) (n = 12).

669 All error bars represent the SEMs. INL, inner nuclear layer; GCL, ganglion cell layer.
670 Scale bars, 50 μm in (B), (D), n.s.: not significant, *$p < 0.05$, **$p < 0.01$, ***$p < 0.001$.
671 unpaired t-test (E),Games-Howell test (C, G, H), Pearson's correlation coefficient (I-K).